RSC Advances

ROYAL SOCIETY OF CHEMISTRY

www.rsc.org/advances

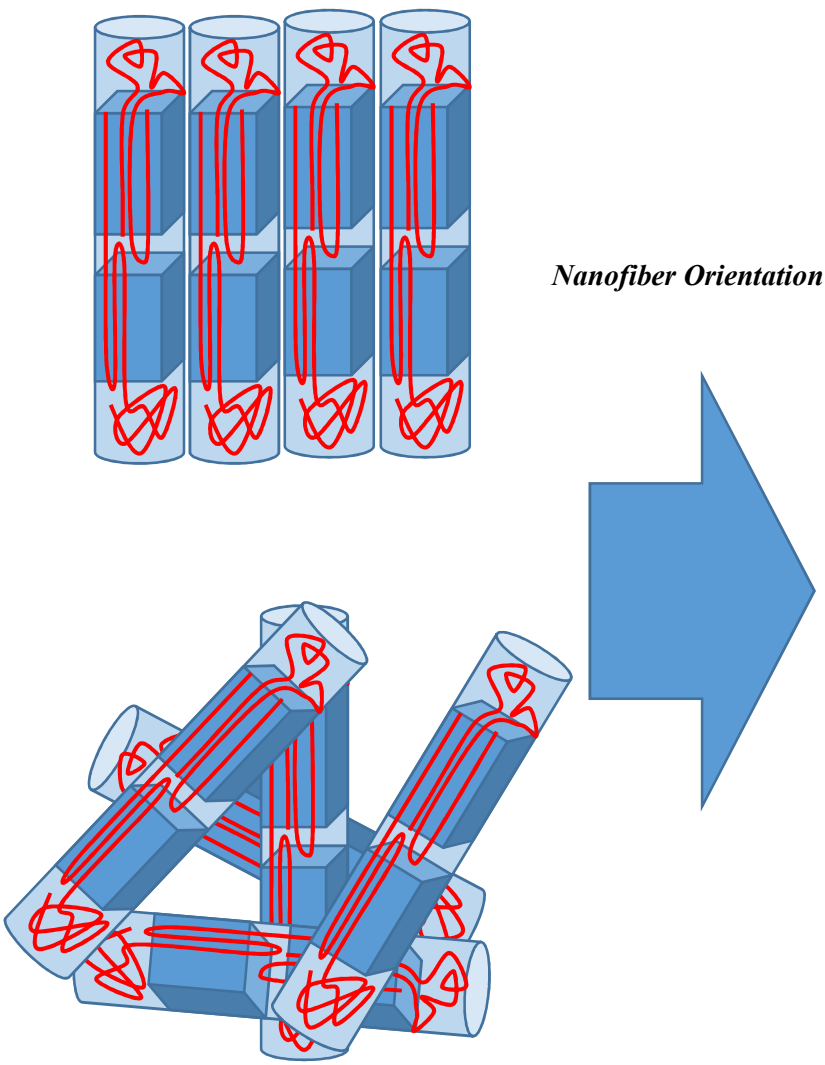

Enhanced Ferroelectric Properties of Electrospun Poly(vinylidene fluoride) Nanofibers by Adjusting Processing Parameters

Mohammad Mahdi Abolhasani[a*], Sara Azimi[a], Hossein Fashandi[b]

[a]Department of Chemical Engineering,University of Kashan, Kashan, Iran
[b]Department of Textile Engineering, Isfahan University of Technology, Isfahan 84156-83111, Iran

Abstract

This contribution investigates the polymorphism evolution of poly(vinylidene flouoride) (PVDF) mats prepared through electrospinning solutions of PVDF in pure N,N-dimethylformamide (DMF) and DMF/acetone mixtures with different weight ratios. To explore the influence of process- as well as solution-related parameters, electrospun webs were characterized with respect to their morphologies and polymorphism features using scanning electron microscopy (SEM), differential scanning calorimetry (DSC), and fourier transfer infrared spectroscopy (FTIR) techniques. . Among various processing parameters, rotation of collecting drum was found to have the pivotal role to enhance the β phase formation. Furthermore, dielectric tests were conducted to disclose the influence of aforementioned parameters on dielectric constant, remnant polarization and coercive field of the mats. It was confirmed the ferroelectric properties of PVDF electrospun mats can be dominantly controlled by orienting fibers in the produced web using a drum collector.

Keywords: electrospinning; orientation; dielectric constant; hysteresis loop

1. INTRODUCTION

Electrospinning has emerged as a powerful and versatile technique allowing nonwoven mats consisting of micro- and/or nano-scale fibers to be fabricated from polymeric solutions and melts [1, 2]. In this process, an electrically charged jet is accelerated toward a grounded collector when the electrical forces overcome the surface tension of the polymer fluid. The orientation of electrospun fibers in collected web is of huge interest to produce polymeric fibrils. These fibrils have gained special attention in manufacturing electronic and photonic devices where anisotropic properties are competent. From another point of view, the fiber orientation favors enhanced electroactivity of ferroelectric polymers [3, 4]. Poly(vinylidene fluoride) (PVDF), one of the ferroelectric polymers, is commonly used in high-tech applications due to its ferro, pyro and piezoelectric activities, dielectric properties, and particularly ease of processability. Depending on the conformations of chains, PVDF exhibits five distinct crystalline phases known as: non-polar α & δ phases, polar β-phase and γ- & ε- phases. The chain conformations in these phases are TGTG', TGTG', TTT, T_3GT_3G' and T_3GT_3G', respectively, which T and G indicate to Trans and Gauche conformations [5-8]. Among these structures, particular attention has been given to the β phase in which chains in all-trans planar zig-zag conformations are packed into an orthorhombic unit cell. The fluorine atoms in β phase end up on one side of the unit cell, resulting in the highest permanent dipole which is responsible for improved electrical properties[5, 9-12].

Recently, a variety of strategies developed to obtain one-dimensional ferroelectric fibers using electrospinning, have promoted the successful design of fiber-based actuators and sensors [3, 13-20]. For instance, Pu *et al.* [20] investigated the piezoelectric actuation of electrospun PVDF fibers and proved that the piezoelectric coefficients of PVDF fibers are two times higher than

the corresponding values associated to their bulk or thin film counterparts. Furthermore, similar promising work [19] focused on the fabrication of nanogenerators using electrospun PVDF fibers demonstrated the high conversion of their produced PVDF fibers. This provides new opportunities for employing these fibers in piezoelectric applications such as wearable 'smart clothes' through which electricity is supplied from strains resulted due to body movements.

Electrospun PVDF fibers have their dipoles naturally aligned in the crystals owing to the extensional forces exerted on the polymer jet during electrospinning. These forces account for the formation of β-crystals where electric dipoles are arisen between the fluorine and hydrogen atoms in individual molecular chains [3, 21-23]. These dipoles and/or ferroelectric features are parallel to the polar axis and also oriented by the static arrangement of the molecular chains. Furthermore, using an external electric field can either orient or reverse these dipoles [24, 25].These facts describe that both ferroelectricity and piezoelectricity in PVDF fibers result from its microstructure and β-crystal formation. Consequently, these properties can be enhanced through the fabrication of PVDF nanofibers with improved crystallinity and increased β-phase content. A rich literature has reported the electrical properties of PVDF nanofibers [3, 14-20]; nevertheless, to the best of our knowledge, a clear picture concerning the effects of processing conditions on developing different polymorphs in PVDF nanofibers and thus their contribution to the nanofibers ferroelectric properties is still missing. From this point of view, this research work aims to discuss about the influence of the electrospinning process parameters, *i.e.* applied voltage, collector type and flow rate, along with solution factors, *i.e.* solvent type and mixture ratio, on the crystalline polymorphism of PVDF nanofibers. The paper also communicates attention towards studying the effects of this polymorphism on remnant polarization, coercive field and dielectric characteristics of PVDF electrospun webs.

2. EXPERIMENTAL

2.1. Materials

PVDF (Solef 1010) with molecular weight of 1×10^5 g/mol was supplied by Solvay, Belgium, and dried in an oven at 70 ºC for 24 h before use. Dimethylformamide (DMF) and acetone were purchased from Merck, Germany, and used as received without further purification.

2.2. Preparation of PVDF nanofibers

Three homogeneous polymer solutions of concentration 20 wt.% were prepared by stirring a given amount of PVDF in DMF or DMF/acetone mixtures (weight ratios of 1:1 and 3:1) at 70 ºC for 24 h. Prior to electrospinning, the prepared solutions were stored in a chamber with constant temperature of 25 ºC to reach equilibrium conditions. Then the solution was loaded in a 5 ml syringe fitted with a steel needle (*i.d.* 0.75 mm diameter). All electrospinning experiments were conducted in an electrospinning apparatus (Nano Azma Co., Iran) with controlled environmental conditions. The temperature of chamber was kept constant at 25 ºC throughout the spinning process. The potential of 13 or 21 kV was applied to the needle using a high voltage power supply. The feeding rate of polymer solution was chosen to be 0.5 or 1 ml/h.

The electrospun fibers were collected either on a static collector or a rotating drum, both located 17 cm away from the needle tip. For the latter case, the rotational speed was adjusted to be 2500 rpm. The operating parameters to produce different classes of PVDF nanofibers are presented in Table 1.

Table 1

2.3. Characterizations techniques

Differential scanning calorimetry (DSC) was conducted using a TA Instrument Q200. Samples were heated from room temperature to 210˚C at a heating rate of 10˚C/min.

Fourier transform infrared spectroscopy (FTIR) was performed to study different polymorphs of the samples using Bruker 70 equipped with ATR unit. For each sample, 64 scans over an absorption band of 500 cm^{-1} to 1500 cm^{-1} were collected with a resolution of 4 cm^{-1}. FTIR spectra were normalized using the absorption value of corresponding peak centered at wavenumber of $cm^{-1.}$

Scanning electron microscopy (SEM) (Zeiss SupraTM 55VP) was employed to investigate the morphology of the electrospun webs. Samples were sputter-coated with a thin layer of gold before imaging. Based on SEM images of produced webs, diameters of fibers were also determined using an image analysis software. The mean and standard deviation values were obtained by readying the diameters of 100 randomly selected fibers. The real (ε') and imaginary (ε'') components of the complex relative permittivity related to PVDF nanofibers were determined with a 4192A Impedance/Gain-Phase Analyzer, using a 16451B dielectric test fixture, both from HP, in the frequency range of 30 to 1.1 $\times 10^6$ Hz at ambient conditions.

Ferroelectric hysteresis loops were measured at ambient temperature with a continuous triangular wave signal electric field. A plot for the electric polarization versus electric field was obtained using an Easy Check 300 (aixACCT Systems GmbH, Germany) equipped with Trek 610E high voltage amplifier T source for measurements at room temperature.

3. RESULTS AND DISCUSSION

3.1. Total crystallinity (X_t) and electroactive β-phase content of PVDF nanofibers

Ferroelectric properties of nanofibers vary with the crystalline structure and polymorphism of PVDF. Strictly speaking, the processing parameters including feeding rate, applied voltage, temperature, spinning distance, collector type (static or rotating drum) and needle diameter greatly contribute to morphology and polymorphism evolution within PVDF nanofibers. In our case, PVDF nanofibers were obtained upon electrospinning the polymer solutions with the same concentration, *i.e.* 20 wt.%, of PVDF in pure DMF or DMF/acetone mixtures on static or rotating collector.

SEM images captured from samples SRE-2 and DRE-2 have been included in Fig. 1. As evident from this figure, rotation of collector leads to an oriented accumulation of nanofibers as displayed in Fig. 1b for sample DRE-2. This clearly introduces employing rotating drum as an effective technique to achieve aligned nanofibers; the same illustrations (not shown here) were observed for other samples electrospun using dynamic collector.

Comparing and analyzing SEM images obtained from a variety of samples demonstrated that regardless of applied voltage, flow rate and feeding rate, degree of nanofibers orientation in the webs electrospun using a rotating drum lies in the range of 70-80%. From another point of view, collecting fibers on the rotating drum is accompanied with a decrease in the average diameters of the electrospun fibers (D<300nm) compared to those deposited on the static collector (D<400nm). This can be interpreted by the fact that the rotational movement of collector acts as an stretching force along the fiber axis which is followed by further thinning of solution jet. Hence, finer fibers are expected.

Figure 1

To further examine the influence of processing parameters on the nanofiber characteristics in terms of fiber crystallinity and polymorphism, the results of FTIR spectroscopy and DSC

techniques were evaluated. The relative content of α and β polymorphs were calculated by Eq. 1[26]:

$$F(\beta) = \frac{X_\beta}{X_\alpha + X_\beta} = \frac{A_\beta}{1.26A_\alpha + A_\beta} \quad (1)$$

where X_α and X_β stand for crystalline mass fractions of α and β phases, respectively; also, A_α and A_β are their corresponding absorption bands at 763 and 840 cm^{-1}, accordingly [27]. The degree of crystallinity (ΔX_c) of each sample was determined using the DSC curves based on the Eq. 2.

$$\Delta Xc = \frac{\Delta H}{x_\alpha \Delta H_\alpha + x_\beta \Delta H_\beta} \quad (2)$$

In Eq. 2, $\Delta H, \Delta H_\alpha$, and ΔH_β are indicate to the melting enthalpy of the sample under consideration and the melting enthalpies of a 100% crystalline sample in the α and β-phases, respectively. Additionally, x_α and x_β correspond to the amount of α- and β-phases in the sample, respectively [28]. In this study, the amounts of 93.07 Jg^{-1} and 103.4 Jg^{-1} [28] were considered for ΔH_α and ΔH_β, respectively. Then, the calculation of x_α and x_β was proceeded using the FTIR measurements based on the Eqs. 3 through 5:

$$A_{762} = K_\alpha^{762}.X_\alpha.t \quad (3)$$

$$A_{1275} = K_\beta^{1275}.X_\beta \cdot t \quad (4)$$

$$A_{835} = (K_\beta^{835} \cdot X_\beta + K_\gamma^{835} \cdot X_\gamma + K_{am}^{835}(1 - X_{total}))t \quad (5)$$

where A_j is the baseline-corrected absorbance at wavenumber j (cm^{-1}), K_i^j is the absorption coefficient at wavenumber j (cm^{-1}) for the phase i, X_i is the mole fraction of the phase i, X_{total} is the total crystallinity, and t indicates to the thickness in micrometers. The total crystallinity of each sample was given using DSC technique and the thickness of the nanofiber web was calculated from the IR absorption band at 1070 cm^{-1} in which the absorption coefficient is independent from the crystalline phase of the polymer and corresponds to: $A_{1070} = 0.095t + 0.07$.

The values obtained for the absorption coefficients, K_{am}^{835}, K_{α}^{762}, K_{γ}^{835}, $K_{\beta}^{1275}$and K_{β}^{835}, were 0.0259, 0.365, 0.150, 0.140 and 0.132 μm^{-1}, , respectively [26].

Normalized FTIR spectrum provides qualitative as well as quantitative information about the structure of all samples (Fig. 2). As evidenced by Fig. 2, there are no discrepancies between the spectra included in this figure, indicating that the processing conditions had slight effects on the crystalline forms of the fibers. β polymorph of PVDF can be easily detected in all samples by absorption band centered at 840 cm^{-1}; however, the peak at 810 cm^{-1} attributed to γ polymorph is not present in the curves. It has been accepted that the peaks centered at 532, 614 and 763 cm^{-1} are commonly appeared as the characteristic α -phase absorption bands for bulk PVDF; whereas, these peaks cannot be distinguished in the spectra recorded for the PVDF fibers electrospun in this research work. This finding can be discussed in relation to the fact that the extensional and elongational forces caused by the electrospinning process have led to the removal of α phase from the PVDF nanofiber structure.

Figure 2

Table 2 represents the effect of electrospinning processing parameters on the fraction of β phase along with the total crystallinity of produced fibers. For example, increasing the applied voltage from 13 to 21 kV has resulted in a small increment in the fraction of β phase. While, the contribution of the collector type to raise F(β) is much more pronounced. However, all processing parameters including applied voltage, feeding rate and collector type had negligible effect on the total crystallinity content of fibers.

Table 2

Generally, it can be inferred that the both process- and solution-related factors such as voltage, feeding rate, solvent ratio and collector type are not held responsible for the amount of the total

crystallinity of fibers. As previously mentioned, slight increase of F(β) upon increment of operating voltage can be considered as another salient result figured out from the data tabulated in Table 2. It seems a reasonable conjecture to suppose that the polymer molecules would become more ordered within the fibers in the presence of the electrostatic field. This result can then be favored by all-trans conformation of the β polymorph. On the contrary, the outcome cited above specifies that collector type is regarded as the most consequential parameter that governs the F(β) content. To put it differently, the collector can effectively alter the microstructure of the nanofibers. Commonly the molecular chains orient based on a balance between deformation and relaxation. Therefore, deformation caused by collector at the final stage of the fiber formation, can be regarded as a crucial issue. The concentration of polymer in the fiber at the latest moment of its formation is higher than that associated to the whipping region and also straight jet section. This fact is due to solvent evaporation and can lead to an increase in the relaxation time of obtained polymeric fiber. At the same time, the collector contributes to the solvent evaporation through increasing the surface/volume ratio of the fiber, inducing further elongation of the jet and subsequent limitation of the relaxation time.

3.2. Ferroelectric Properties of PVDF nanofibers

Low-field dielectric spectroscopy results of electrospun SRE and DRE mats (real part (ε_r') and imaginary part (ε_r") of relative permittivity) at room temperature as a function of frequency are shown in Figure 3, other samples not shown here revealed the same trend. Comparing ε_r' curves obtained for different processing conditions throughout the entire frequency range, it is found that the samples collected on the rotating drum have exhibited ε_r' with the values about 40% higher than those related to the samples obtained while the collector was static. However, neither a mere increasing trend nor a decreasing one is distinguished in the amount of ε_r' upon the

variation of parameters including applied voltage, feeding rate, and solvent type. This finding can be explained by the previous results which confirmed that increment of applied voltage has caused the β phase content to increase but the total crystallinity to decrease in some cases. Consequently, we didn't observe any clear trend in ε_r' by increasing the applied voltage. As expected, when a rotating drum is applied during the electrospinnig process, fibers as aligned. Also, chain orientation in the amorphous region of the mat is improved in the fiber direction and thus packing is developed. It is known that the dielectric properties of PVDF are anisotropic; namely, the dielectric constants perpendicular and parallel to the chain axes are different[29, 30]. Therefore, application of an external electric field perpendicular to the sample surface led to the orientation of the dipole moments favored by chain orientation which is parallel to the sample. Hence, collector type can effectively govern the dielectric constant because component dipole moments perpendiculars to the chain axis are oriented in dynamic collector in comparison with the static one as shown schematically in Figure 4.

Figure 3

Figure 4

Figure 3.b shows that loss dielectric constants related to the static and dynamic collectors have relaxation at low and high frequencies, respectively. The relaxation peak around 100 Hz corresponds to the dipole relaxation, laterally the chain axes [30, 31] and the relaxation peak around 10^6 Hz is assigned to the amorphous dipoles[32-34].It is noteworthy to mention that the relaxation peak around 100 Hz is in the power frequency range ;therefore, mats prepared by static collector are not suitable for high energy density and low loss dielectrics. While, electrospun mats supplied by dynamic collector with a parallel crystal orientation have superior dielectric loss properties since increasing the temperature will shift the relaxation peak at 10^6 Hz

to the higher frequencies[32]. In order to demonstrate better understanding of this behavior, ε" were measured as a function of temperature at three different values for DRE-1 sample. As can be observed in Figure 5, the relaxation peak for this sample has shifted to the higher frequencies upon the temperature growth from -20°C to 20°C. This is related to β relaxation, which is associated with the localized motions of side groups in the glassy state.

Figure 5

Figure 6

Besides, the high-field behaviors of electrospun SRE-1 and DRE-1 mats were investigated using unipolar hysteresis loops (Figure 6). Remnant polarization and coercive field of the mat can be obtained from the hysteresis loop. The mat electrospun using dynamic collector has a stable remnant polarization which is50% higher than that of the sample prepared by static collector. In contrast, replacement of the static collector with the rotating one has caused the coercive field of the mat to reduce about 20%. Table 3 compares the remnant polarization and coercive field of both SRE and DRE samples. The higher remnant polarization of the samples prepared by dynamic drum compared to static collector is due to the orientation of the mat chains, as crystallinity did not increase with collector type (verified by Table 2). This result can be clarified by the dynamic collection of the fibers which leads the chain in the crystalline phases to orient in the direction of the fibers. Thus, dipoles will form perpendicular to the fiber direction. Then, the orientation of the nanofibers makes poling occur easier, as an electric field is exerted perpendicular to the film surface. Similarly, this phenomenon will appear in the amorphous phase of the polymeric mats. These effects also tend to lower the coercive field of the electrospun mats collected on the dynamic drum.

Table 3

4. Conclusion

The main goal of this study was to vary the processing and solution parameters such as flow rate, applied voltage, solvents type, mixture ratio and collector type in the experiments and describe the dependence of nanofiber morphology, total crystallinity, polymorphism, and ferroelectric properties of PVDF fibers on the mentioned factors. For the successful evaluation of these issues, different samples were prepared under various conditions. It was depicted that the percent of orientation for the samples prepared by rotating drum are between 70-80% and almost independent of applied voltage, fellow rate, and feeding rate. Furthermore, average diameters of the samples prepared by rotating drum (D<300nm) were lower than those related to the static collector (D<400nm). Another result has dealt with the polymorphism investigation, pointing out that increasing the applied voltage from 13 to 21 kV demonstrates small increase in the fraction of β phase; while, collector type has a much considerable effect on F(β). An analogy between the performances of two kinds of collectors revealed that the fraction of β phase will increase, if a rotating drum is employed instead of a static collector in the electrospinning procedure.

As a consequence of comparing dielectric constants obtained at different processing conditions, using rotating collector was known to increase (about 40%) the amount of ε_r'corresponding to the samples prepared by static collector throughout the entire frequency range. However, applied voltage, feeding rate and solvent type didn't show clear increasing or decreasing trend in the level of ε_r'. Loss dielectric constant measurements showed relaxation peak at low and high frequencies for static and dynamic collector, respectively, proving the effects of fiber orientation on loss dielectric behavior. Also, the remnant polarization and coercive field of the electrospun mats using dynamic drum were 50% higher and 20% lower than those of sample obtained by static collector, respectively.

Acknowledgment

The corresponding author thanks financial support from the Iran National Science Foundation (INSF) and anonymous reviewers for their stimulating suggestions and remarks.

References

1. Huang, Z.-M., et al., *A review on polymer nanofibers by electrospinning and their applications in nanocomposites.* Composites science and technology, 2003. 63(15): p. 2223-2253.
2. Persano, L., et al., *Industrial upscaling of electrospinning and applications of polymer nanofibers: a review.* Macromolecular Materials and Engineering, 2013. 298(5): p. 504-520.
3. Baji, A., et al., *Electrospinning induced ferroelectricity in poly (vinylidene fluoride) fibers.* Nanoscale, 2011. 3(8): p. 3068-3071.
4. Su, R., et al., *Polarity-induced ferroelectric crystalline phase in electrospun fibers of poly (vinylidene fluoride)/polyacrylonitrile blends.* Journal of Materials Research, 2012. 27(10): p. 1389-1398.
5. Abolhasani, M.M., M. Naebe, and Q. Guo, *A new approach for mechanisms of ferroelectric crystalline phase formation in PVDF nanocomposites.* Physical Chemistry Chemical Physics, 2014. 16(22): p. 10679-10687.
6. Abolhasani, M.M., et al., *Influence of miscibility phenomenon on crystalline polymorph transition in poly (vinylidene fluoride)/acrylic rubber/clay nanocomposite hybrid.* PloS one, 2014. 9(2): p. e88715.
7. Abolhasani, M.M., et al., *Crystalline structures and α→ β and γ polymorphs transformation induced by nanoclay in PVDF-based nanocomposite.* NANO, 2014. 9(06).
8. Baqeri, M., et al., *Influence of processing conditions on polymorphic behavior, crystallinity, and morphology of electrospun poly (VInylidene fluoride) nanofibers.* Journal of Applied Polymer Science, 2015. 132(30).
9. Xu, D., Y. Bin, and K. Tashiro, *Detailed analysis of temperature dependences of spherulite morphology and crystallite orientation of poly (vinylidene fluoride) via a combinatorial method.* Journal of Polymer Science Part B: Polymer Physics, 2015. 53(4): p. 253-261.
10. Sharma, M., G. Madras, and S. Bose, *Process induced electroactive β-polymorph in PVDF: effect on dielectric and ferroelectric properties.* Physical Chemistry Chemical Physics, 2014. 16(28): p. 14792-14799.
11. Miao, J., et al., *Molecular dynamics simulations of relaxation in stretched PVDF nanofibers.* Polymer, 2015. 56: p. 482-489.
12. Abolhasani, M.M., et al., *A facile method to enhance ferroelectric properties in PVDF nanocomposites.* RSC Advances, 2015. 5(29): p. 22471-22479.
13. Song, Y., et al., *Enhanced dielectric and ferroelectric properties induced by dopamine-modified BaTiO3 nanofibers in flexible poly (vinylidene fluoride-trifluoroethylene) nanocomposites.* J. Mater. Chem., 2012. 22(16): p. 8063-8068.
14. Liu, Z., et al., *Piezoelectric properties of PVDF/MWCNT nanofiber using near-field electrospinning.* Sensors and Actuators A: Physical, 2013. 193: p. 13-24.
15. Nunes-Pereira, J., et al., *Energy harvesting performance of piezoelectric electrospun polymer fibers and polymer/ceramic composites.* Sensors and Actuators A: Physical, 2013. 196: p. 55-62.

16. Ahn, Y., et al., *Enhanced Piezoelectric Properties of Electrospun Poly (vinylidene fluoride)/Multiwalled Carbon Nanotube Composites Due to High β-Phase Formation in Poly (vinylidene fluoride).* The Journal of Physical Chemistry C, 2013. 117(22): p. 11791-11799.
17. Baji, A., et al., *Microstructure development in electrospun carbon nanotube reinforced polyvinylidene fluoride fibers and its influence on tensile strength and dielectric permittivity.* Composites science and technology, 2013. 88: p. 1-8.
18. Gasparini, T.M., et al., *Processing and characterization of oriented electrospun poly (vinylidene fluoride) mats.* Journal of Polymer Science Part B: Polymer Physics, 2012. 50(18): p. 1304-1311.
19. Chang, C., et al., *Direct-write piezoelectric polymeric nanogenerator with high energy conversion efficiency.* Nano letters, 2010. 10(2): p. 726-731.
20. Pu, J., et al., *Piezoelectric actuation of direct-write electrospun fibers.* Sensors and Actuators A: Physical, 2010. 164(1): p. 131-136.
21. Fashandi, H., A. Yegane, and M.M. Abolhasani, *Interplay of liquid-liquid and solid-liquid phase separation mechanisms in porosity and polymorphism evolution within poly (vinylidene fluoride) nanofibers.* Fibers and Polymers, 2015. 16(2): p. 326-344.
22. Baji, A., Y.W. Mai, and S.C. Wong, *Effect of fiber size on structural and tensile properties of electrospun polyvinylidene fluoride fibers.* Polymer Engineering & Science, 2014.
23. Xing, C., et al., *Effect of a Room-Temperature Ionic Liquid on the Structure and Properties of Electrospun Poly (vinylidene fluoride) Nanofibers.* ACS applied materials & interfaces, 2014. 6(6): p. 4447-4457.
24. Lovinger, A.J., *Ferroelectric polymers.* Science, 1983. 220(4602): p. 1115-1121.
25. Humphreys, J., et al., *A study of the drawing behavior of polyvinylidene fluoride.* Journal of applied polymer science, 1985. 30(10): p. 4069-4079.
26. Martins, P., A. Lopes, and S. Lanceros-Mendez, *Electroactive phases of poly (vinylidene fluoride): Determination, processing and applications.* Progress in polymer science, 2014. 39(4): p. 683-706.
27. Andrew, J. and D. Clarke, *Effect of electrospinning on the ferroelectric phase content of polyvinylidene difluoride fibers.* Langmuir, 2008. 24(3): p. 670-672.
28. Benz, M. and W.B. Euler, *Determination of the crystalline phases of poly (vinylidene fluoride) under different preparation conditions using differential scanning calorimetry and infrared spectroscopy.* Journal of Applied Polymer Science, 2003. 89(4): p. 1093-1100.
29. Miyamoto, Y., H. Miyaji, and K. Asai, *Anisotropy of dielectric relaxation in crystal form II of Poly (vinylidene fluoride).* Journal of Polymer Science: Polymer Physics Edition, 1980. 18(3): p. 597-606.
30. Marcus, M., *Orientation effects on dielectric and piezoelectric properties of polyvinylidene fluoride films.* Electrical Insulation, IEEE Transactions on, 1986(3): p. 519-523.
31. Miyamoto, T. and K. Shibayama, *Free-volume model for ionic conductivity in polymers.* Journal of applied physics, 1973. 44(12): p. 5372-5376.
32. Furukawa, T. and G. Johnson, *Measurements of ferroelectric switching characteristics in polyvinylidene fluoride.* Applied Physics Letters, 1981. 38(12): p. 1027-1029.
33. Mijovic, J., J.-W. Sy, and T. Kwei, *Reorientational dynamics of dipoles in poly (vinylidene fluoride)/poly (methyl methacrylate)(PVDF/PMMA) blends by dielectric spectroscopy.* Macromolecules, 1997. 30(10): p. 3042-3050.
34. Hahn, B., J. Wendorff, and D.Y. Yoon, *Dielectric relaxation of the crystal-amorphous interphase in poly (vinylidene fluoride) and its blends with poly (methyl methacrylate).* Macromolecules, 1985. 18(4): p. 718-721.

Table 1. Electrospinning parameters used to prepare different nanofibers

Dynamic collector sample code	Static collector sample code	DMF/acetone weight ratio	Voltage (kV)	Flow rate (ml/h)
DRE-1	SRE-1	1/0	13	0.5
DRE-2	SRE-2	1/0	13	1
DRE-3	SRE-3	1/0	21	0.5
DRE-4	SRE-4	1/0	21	1
DTE-1	STE-1	3/1	13	0.5
DTE-2	STE-2	3/1	13	1
DTE-3	STE-3	3/1	21	0.5
DTE-4	STE-4	3/1	21	1
DSE-1	SSE-1	1/1	13	0.5
DSE-2	SSE-2	1/1	13	1
DSE-3	SSE-3	1/1	21	0.5
DSE-4	SSE-4	1/1	21	1

Table 2. Fraction of β phase (F(β)) and total crystallinity (X_{total}) of different produced PVDF nanofibers			
	flow rate (ml/h)	F(β) [voltage =13 kV]	F(β) [voltage = 21 kV]
Samples SRE	0.5	0.59 (X_{total} = 0.50)	0.61 (X_{total} = 0.50)
	1	0.61 (X_{total} = 0.54)	0.63 (X_{total} = 0.53)
Samples DRE	0.5	0.80 (X_{total} = 0.53)	0.83 (X_{total} = 0.55)
	1	0.79 (X_{total} = 0.59)	0.82 (X_{total} = 0.49)
Samples STE	0.5	0.61 (X_{total} = 0.44)	0.62 (X_{total} = 0.47)
	1	0.63 (X_{total} = 0.43)	0.63 (X_{total} = 0.41)
Samples DTE	0.5	0.83 (X_{total} = 0.41)	0.84 (X_{total} = 0.49)
	1	0.84 (X_{total} = 0.45)	0.81 (X_{total} = 0.54)
Samples SSE	0.5	0.58 (X_{total} = 0.43)	0.60 (X_{total} = 0.45)
	1	0.62 (X_{total} = 0.43)	0.61 (X_{total} = 0.55)
Samples DSE	0.5	0.84 (X_{total} = 0.42)	0.83 (X_{total} = 0.42)
	1	0.82 (X_{total} = 0.47)	0.82 (X_{total} = 0.46)

Table 3. comparison of remnant polarization and coercive field for samples electrospun using static collector or rotating drum

Rotating collector	remnant polarization (mC/m^2)	coercive field (MV/m)	Static collector	remnant polarization (mC/m^2)	coercive field (MV/m)
DRE-1	51	62	SRE-1	35	75
DRE-2	53	64	SRE-2	35	76
DRE-3	60	71	SRE-3	39	80
DRE-4	62	72	SRE-4	40	80

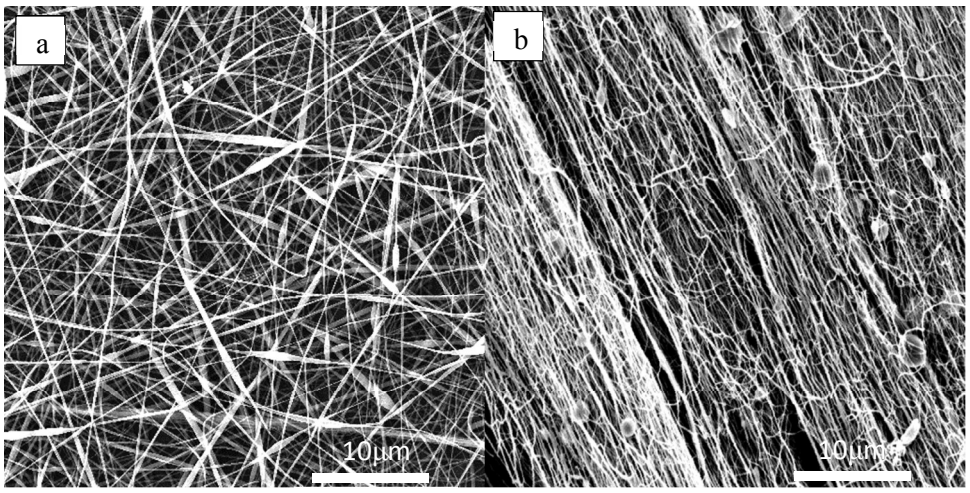

Figure 1. SEM images of electrospun PVDF nanofibers electrospun from PVDF/DMF solution (applied voltage:13 kV and flow rate: 1 mL/h) using a) static collector b) rotating collector (samples SRE-2 and DRE-2).

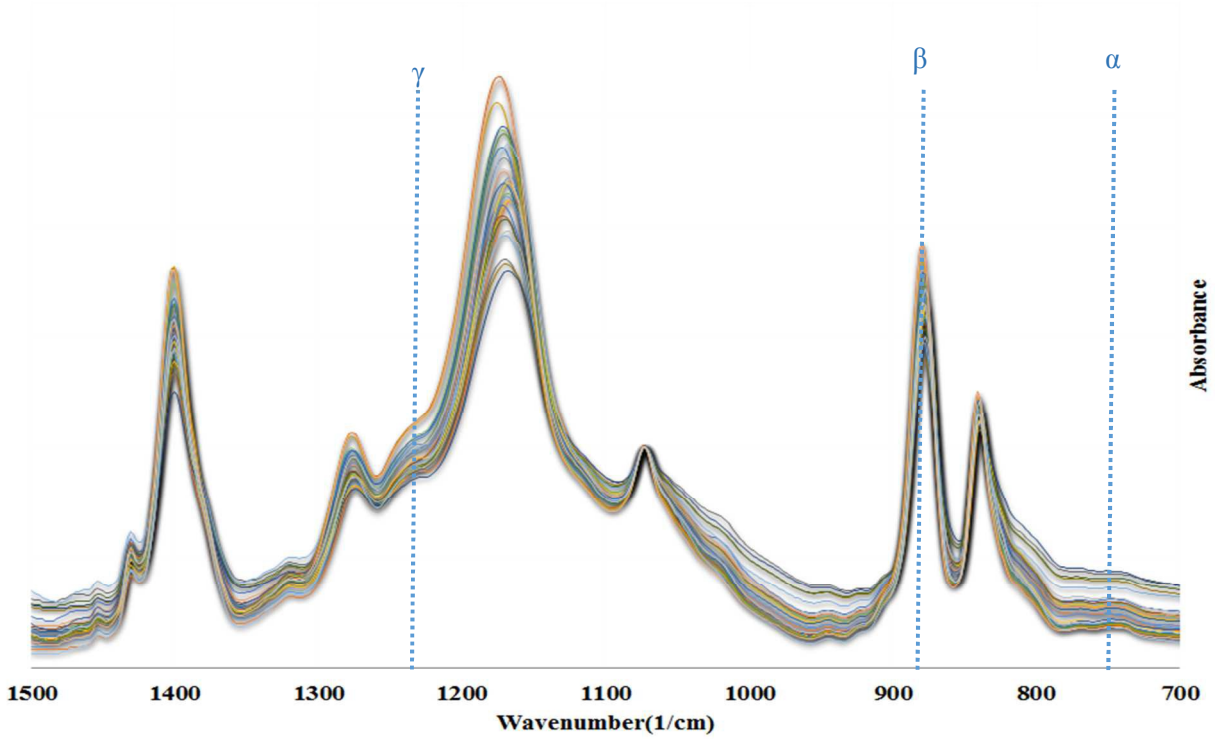

Figure 2. FTIR spectra of all electrospun PVDF nanofibers sample.

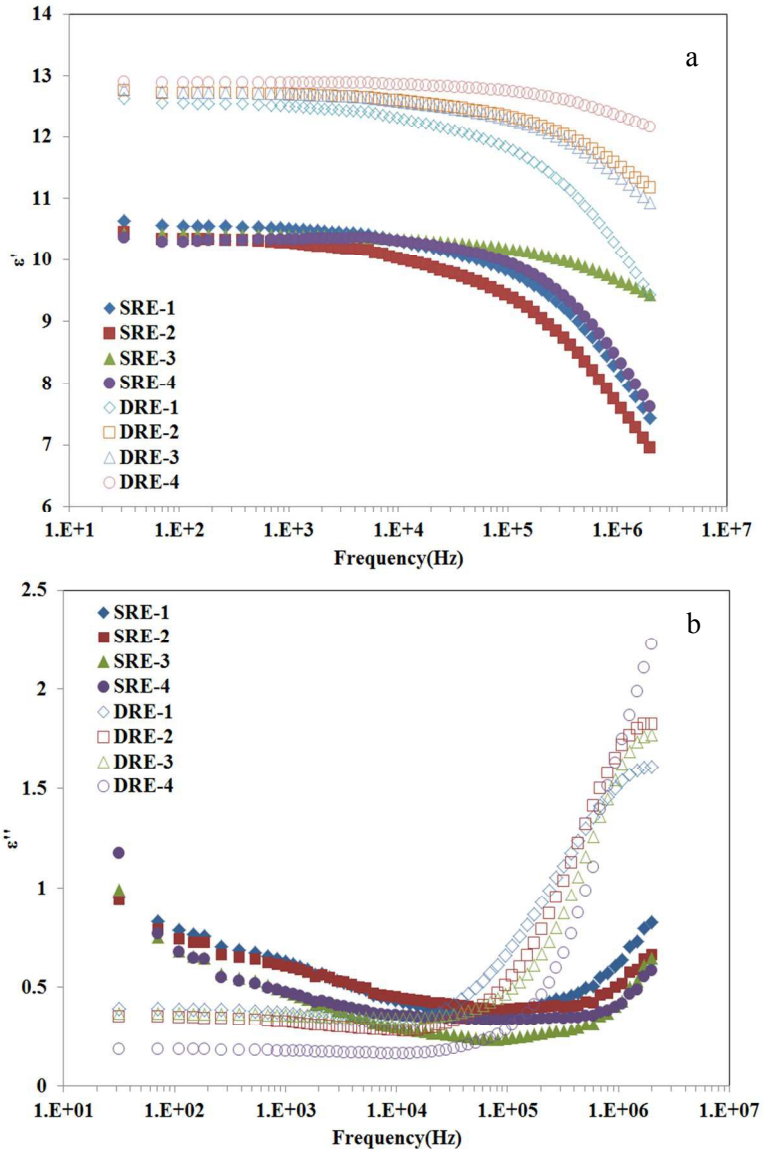

Figure 3. (a) Real part (ε_r') and (b) imaginary part (ε_r") of relative permittivity measured at room temperature as a function of frequency for samples SRE and DRE .

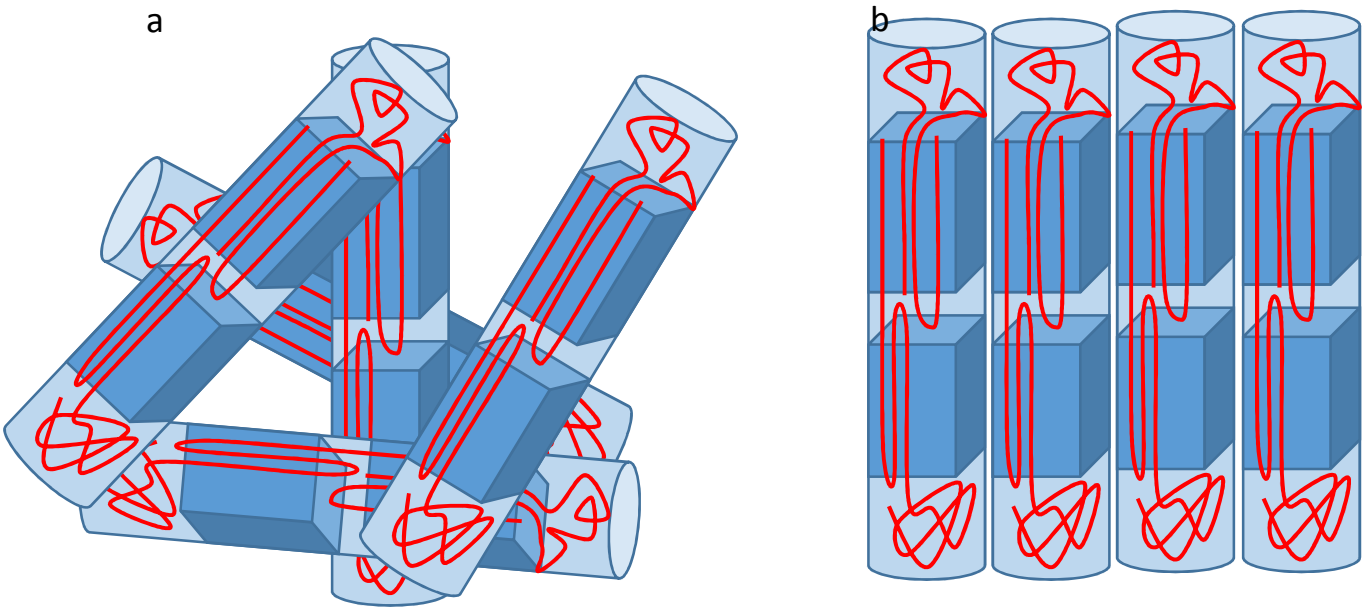

Figure 4. Schematic representation of the contribution of collector type to orient PVDF crystals: (a) static collector and (b) dynamic collector (Adapted from ref. 15).

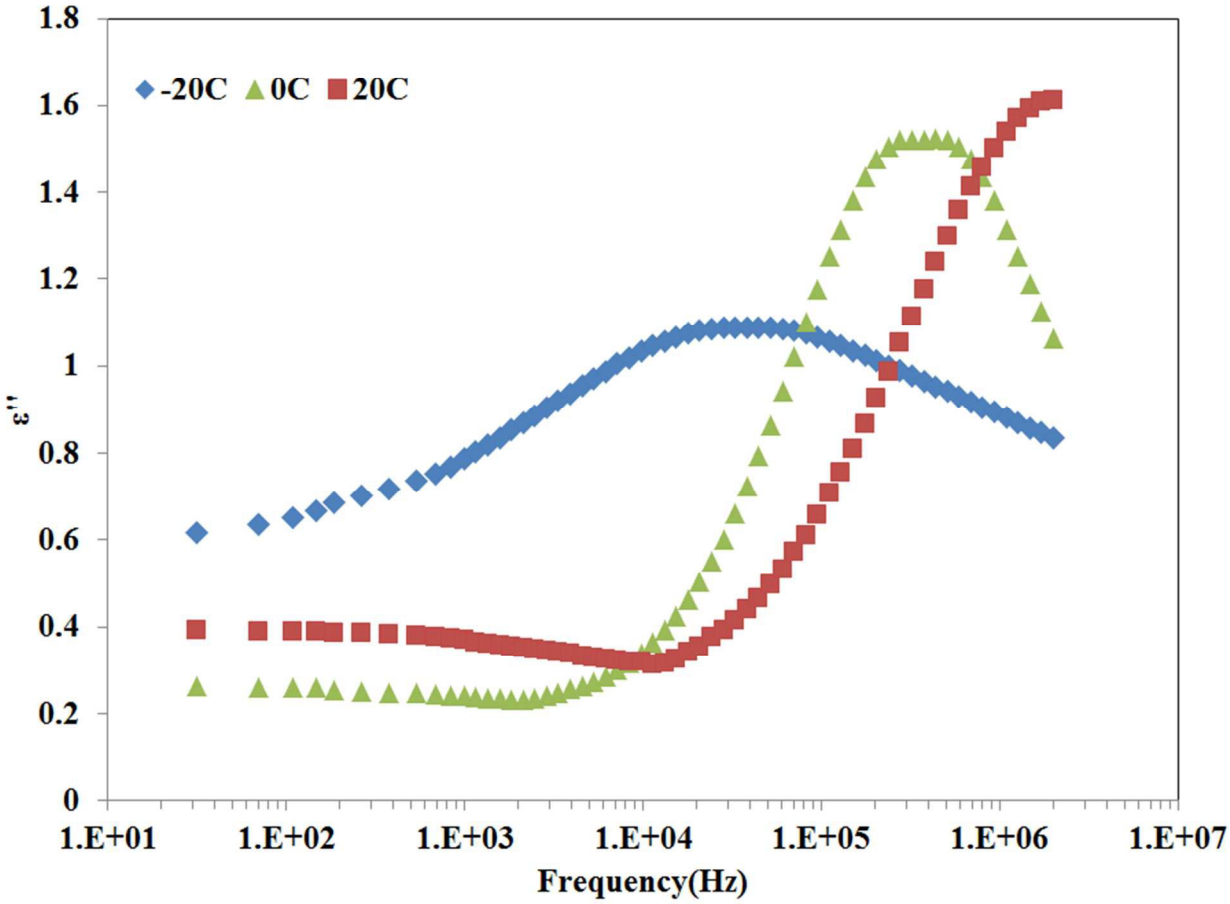

Figure5. Loss dielectric vs. frequency at different temperatures for sample DRE-1.

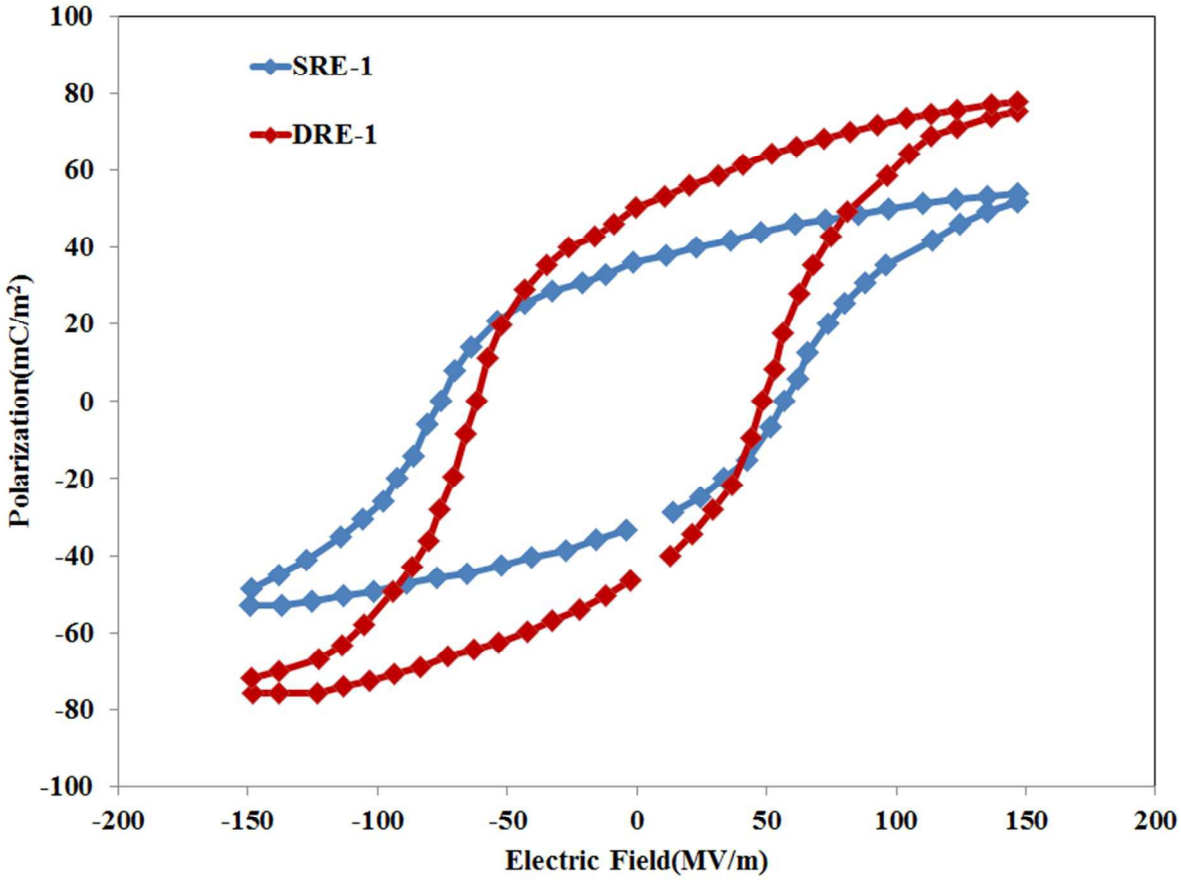

Figure 6. P-E hysteresis loop for the DRE-1 and SRE-1 electrospun PVDF mats.